A&A 518, L92 (2010)
DOI: 10.1051/0004-6361/201014618
© ESO 2010

Astronomy & Astrophysics
Special feature

Herschel: the first science highlights

Letter to the Editor

A *Herschel*⋆ study of the properties of starless cores in the Polaris Flare dark cloud region using PACS and SPIRE

D. Ward-Thompson[1], J. M. Kirk[1], P. André[2], P. Saraceno[3], P. Didelon[2], V. Könyves[2], N. Schneider[2], A. Abergel[4], J.-P. Baluteau[5], J.-Ph. Bernard[6], S. Bontemps[2], L. Cambrésy[7], P. Cox[8], J. Di Francesco[9], A. M. Di Giorgio[3], M. Griffin[1], P. Hargrave[1], M. Huang[10], J. Z. Li[10], P. Martin[11], A. Men'shchikov[2], V. Minier[2], S. Molinari[3], F. Motte[2], G. Olofsson[12], S. Pezzuto[11], D. Russeil[6], M. Sauvage[2], B. Sibthorpe[13], L. Spinoglio[3], L. Testi[14], G. White[15,16], C. Wilson[17], A. Woodcraft[13], and A. Zavagno[5]

(Affiliations are available in the online edition)

Received 31 March 2010 / Accepted 10 May 2010

ABSTRACT

The Polaris Flare cloud region contains a great deal of extended emission. It is at high declination and high Galactic latitude. It was previously seen strongly in IRAS Cirrus emission at 100 microns. We have detected it with both PACS and SPIRE on *Herschel*. We see filamentary and low-level structure. We identify the five densest cores within this structure. We present the results of a temperature, mass and density analysis of these cores. We compare their observed masses to their virial masses, and see that in all cases the observed masses lie close to the lower end of the range of estimated virial masses. Therefore, we cannot say whether they are gravitationally bound prestellar cores. Nevertheless, these are the best candidates to be potential prestellar cores in the Polaris cloud region.

Key words. stars: formation – ISM: clouds – dust, extinction

1. Introduction

In this paper we present observations, performed with the ESA *Herschel* Space Observatory (Pilbratt et al. 2010), of the Polaris Flare region. In particular we use the large collecting area and powerful science payload of *Herschel* to perform imaging photometry using the PACS (Poglitsch et al. 2010) and SPIRE (Griffin et al. 2010) instruments. These observations were carried out as part of the guaranteed-time key programme to map most of the Gould Belt star-forming regions with *Herschel* (André et al. 2010). The Polaris Flare was first detected in HI as a spur of gas that appears to rise more than 30° out of the Galactic plane. This region is an area rich in IRAS cirrus emission (e.g. Low et al. 1984), and is sometimes known as the Polaris Cirrus cloud. It was mapped in CO by Heithausen & Thaddeus (1990). On the large scale this cloud appears to merge with the Cepheus Flare cloud (e.g. Kirk et al. 2009), and both clouds extend to high Galactic latitude.

One of the denser regions in the cloud is known as molecular cloud 123.5+24.9, or MCLD 123.5+24.9 (e.g. Bensch et al. 2003) – hereafter MCLD 123 – at a distance of 150 pc (Bensch et al. 2003). It shows strong extended IRAS 100-μm emission and is generally believed to be gravitationally unbound with a mass of ~18–32 $M_\odot$ (Grossmann et al. 1990; Bensch et al. 2003). A CO study by Falgarone et al. (1998) revealed a curved filament in MCLD 123 in ^{13}CO and C^{18}O – both in the $J = 2$–1 transition. This filament is also apparent in some narrow velocity channels in the same transition of ^{12}CO (Falgarone et al. 1998).

There is one IRAS source in the region, IRAS 01432+8725. This is listed in the IRAS catalogue as having a flux density at 100 μm of 2.88 Jy, but only upper limits at the other IRAS wavebands. There is also one *Spitzer* source that was only detected at a wavelength of 24 μm at coordinates RA (2000) = $01^h58^m27.5^s$, Dec (2000) = +87°40′07″. It has a peak flux density at 24 μm of 1.3 mJy/beam, where the *Spitzer* beam at this wavelength is 7 arcsec. This detection lies in a *Spitzer* calibration field in an unpublished archival dataset (AOR 33136386).

2. Observations

The SPIRE/PACS parallel-mode science demonstration observations of the Polaris cloud were performed on 2009 October 23 (Operation Day 162) at wavelengths of 70 μm and 160 μm with PACS, and at 250 μm, 350 μm and 500 μm with SPIRE. The 70- and 160-μm ~6 deg^2 scan map was taken with 60 arcsec/s scanning speed. The field was observed twice with both instruments by performing cross-linked scans in two nearly orthogonal scan directions. The combination of nominal and orthogonal coverages reduced the effects of $1/f$ noise and better preserved spatial resolution. The SPIRE data were reduced using HIPE version 2.0 and the pipeline scripts delivered with this version. These scripts were modified, e.g. observations that were taken during the turnaround of the satellite were included. A median baseline (HIPE default) was applied to the maps and the "naive mapper" was used for map making.

The PACS data were reduced with HIPE 3.0.455 provided by the *Herschel* Science Center (HSC). We used file version 1 flat-fielding and responsivity in the calibration tree, instead of the built-in version 3. Therefore the error in the final reduced flux scale was corrected manually with the corresponding correction

⋆ *Herschel* is an ESA space observatory with science instruments provided by European-led Principal Investigator consortia and with important participation from NASA.

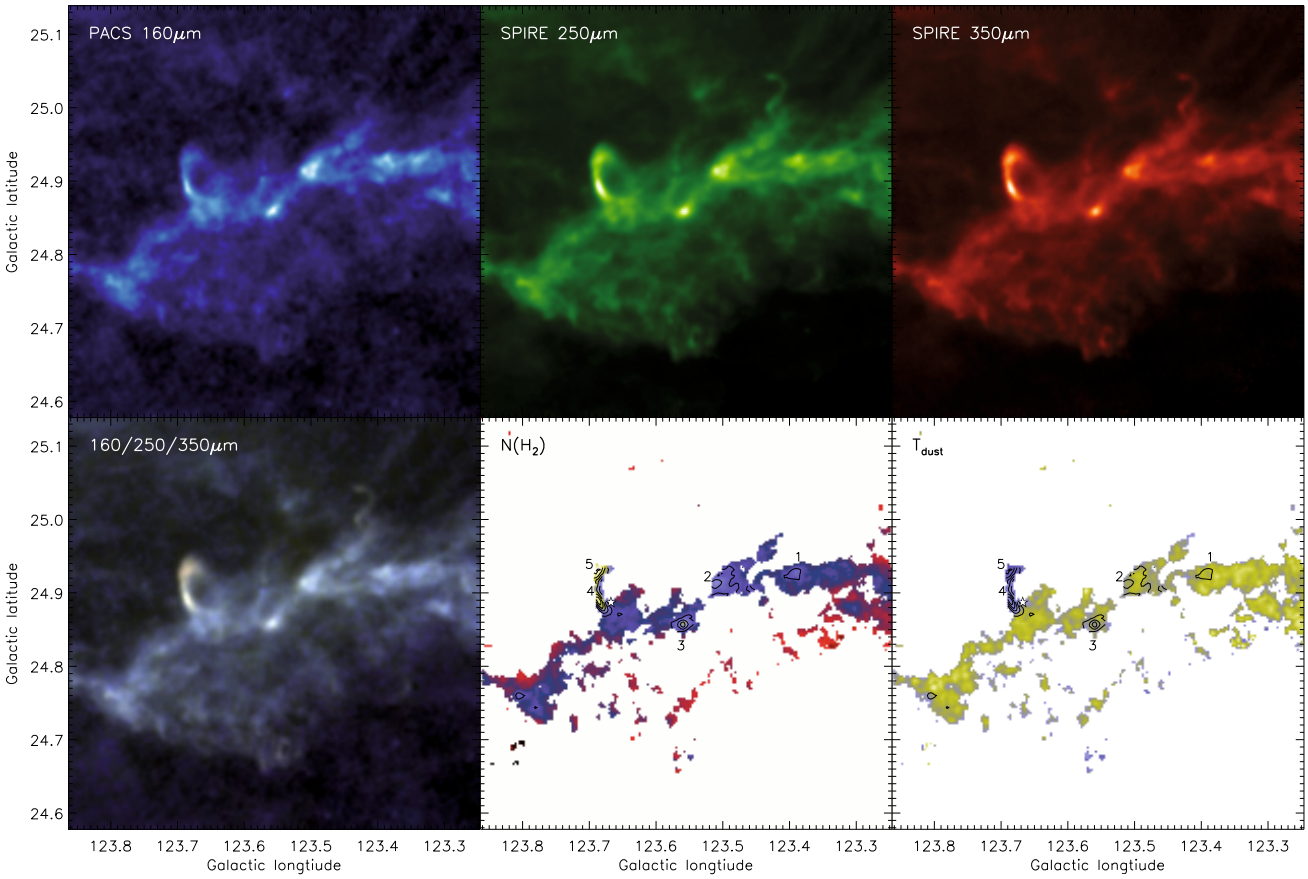

Fig. 1. The densest part of the Polaris Flare region at some of the observed wavebands. *Upper row*: 160 μm from PACS, and 250 μm and 350 μm from SPIRE. *Lower row*: false-colour image (where 160 μm is shown in blue, 250 μm is shown in green, and 350 μm is shown in red), column density map (where red is <4, blue is 4–8, and yellow is >8 $\times$ 10^{21} cm^{-2}), and colour temperature map (where blue is 10–11 K and yellow is 12–13 K). The contour levels on the column density map start at 4 $\times$ 10^{21} cm^{-2}, and the interval between successive contours is 1.5 $\times$ 10^{21} cm^{-2}. The same contours are repeated on the temperature map for ease of location. Five sources are seen above a column density of 4 $\times$ 10^{21} cm^{-2}. These are labelled cores 1–5 (in order of increasing RA) on the last two panels and are discussed in the text. The loop (loop 1) discussed in the text (containing cores 4 & 5) is clearly visible in all images. The reddest features on the false-colour image are the coldest, and the loop shows up clearly as redder than the surroundings. Likewise in the temperature map, the loop shows up as blue, indicating that it is the coldest feature on the map. The position of the IRAS source (IRAS 01432+8725) is marked with a star on the last two panels (adjacent to core 4).

values in the PACS wavelengths. Standard steps of the default pipeline were applied for data reduction starting from (level 0) raw data. Multi-resolution median transform (MMT) deglitching and second order deglitching were also applied. Baselines were subtracted from the level 1 data by high-pass filtering with a ~1° filter width, avoiding obvious sources, whilst the full leg length was 2.5° in the parallel mode.

The PACS data of this field include transients of unknown origin after each calibration block, which seriously affected the ensuing frames. We processed these observations using data-masking and a narrower high-pass filter width than the image size in order to mitigate the calibration block artifacts. In this process, we may have removed spatial scales larger than the filter widths. The final PACS maps were created using the HIPE "MADmap" mapping method projected to the 3.2 and 6.4 arcsec/pixel size for 70 and 160 μm data, respectively.

3. Results

The Polaris Flare dark cloud region was observed at five wavelengths – 70, 160, 250, 350 and 500 μm. Figure 1 shows some of the main results. Only the densest part of the mapped region is shown. The area shown is just over half a degree square. The upper row of Fig. 1 shows the data from three of the wavebands: 160 μm from PACS; and 250 μm and 350 μm from SPIRE. The data have been smoothed to a common resolution of 24 arcsec, the approximate resolution of the 350-μm data. The images have also been re-gridded onto 10 $\times$ 10 arcsec pixels.

The lower row of Fig. 1 shows some images derived from the raw data: a false-colour image; a column density map; and a colour temperature map. The contours on the column density map are at 4, 5.5, and 7 $\times$ 10^{21} cm^{-2}. These are repeated on the temperature map to assist in source location. The Polaris cloud is clearly seen, and the raw data show a complex structure that is broadly similar at all wavebands. There are a number of filamentary structures seen in the data, with a few brighter cores embedded in the cloud.

There is a filamentary loop seen in all images that is centred roughly at Galactic coordinates l = 123.67, b = +24.89 – RA(2000) = 01^{h}58^{m}, Dec(2000) = 87°40′. We here label this feature loop 1. This is the same curved filament as was seen by Falgarone et al. (1998) in ^{13}CO. They interpreted this as an edge of a cloud core. However, in the continuum we see it is clearly a loop with no filled centre. It was also detected in various transitions by Grossman & Heithausen (1992).

There is also a filament with an apparent bifurcation at roughly Galactic coordinates l = 123.48, b = +24.90 – RA(2000) = 01^{h}42^{m}, Dec(2000) = 87°43′. A bright core region is seen at the head of this bifurcation, which may be broken up

Table 1. The physical properties of the cores.

Parameter	Core 1	Core 2	Core 3	Core 4	Core 5
Galactic longitude (2000)	123.388	123.511	123.559	123.687	123.690
Galactic latitude (2000)	+24.928	+24.915	+24.856	+24.894	+24.931
Right ascension (2000)	$01^h34^m01.9^s$	$01^h44^m51.6^s$	$01^h47^m40.8^s$	$01^h59^m42.7^s$	$02^h00^m58.7^s$
Declination (2000)	+87°45′42″	+87°43′35″	+87°39′33″	+87°39′53″	+87°41′58″
Distance (pc)	150	150	150	150	150
Radius (pc)	0.023	0.035	0.032	0.035	0.034
FWHM (pc)	0.023	0.039	0.027	0.042	0.038
$F^{\rm int}_{70\ \mu{\rm m}}$ (Jy)	<0.18	<0.18	<0.18	<0.18	<0.18
$F^{\rm int}_{160\ \mu{\rm m}}$ (Jy)	4.26 ± 0.07	10.19 ± 0.07	7.56 ± 0.07	7.63 ± 0.07	5.44 ± 0.07
$F^{\rm int}_{250\ \mu{\rm m}}$ (Jy)	6.74 ± 0.04	16.77 ± 0.04	13.10 ± 0.04	15.35 ± 0.04	13.26 ± 0.04
$F^{\rm int}_{350\ \mu{\rm m}}$ (Jy)	3.61 ± 0.02	8.98 ± 0.02	7.27 ± 0.02	9.05 ± 0.02	8.50 ± 0.02
$F^{\rm int}_{500\ \mu{\rm m}}$ (Jy)	1.72 ± 0.02	4.33 ± 0.02	3.50 ± 0.02	4.53 ± 0.02	4.40 ± 0.02
Temperature (K)	12 ± 1	12 ± 1	12 ± 1	11 ± 1	10 ± 1
$N(H_2)_{\rm peak}$ ($\times10^{21}$ cm^{-2})	6 ± 3	7 ± 3	9 ± 4	13 ± 5	13 ± 5
Mass ($M_\odot$)	0.1	0.3	0.3	0.4	0.5
$n(H_2)_{\rm mean}$ (cm^{-3})	~5×10^4	~4×10^4	~4×10^4	~5×10^4	~7×10^4
$M_{\rm vir}$ ($M_\odot$)	~0.3–0.5	~1.0–1.5	~1.0–1.5	~1.0–1.5	~1.0–1.5

Notes. The Galactic latitude and longitude, as well as right ascension and declination, are listed, along with the assumed distance. The radius of each core was measured by taking the column density map in Fig. 1 and measuring the equivalent radius of the contour that encircled a column density of 4×10^{21} cm^{-2}, and this radius is given in pc. The full-width at half maximum (*FWHM*) is the geometric mean *FWHM* measured on the peak of each source. The integrated flux density within this contour at each of the *Herschel* wavelengths is listed in Jy. The absolute uncertainty in the flux densities is ±15%. As described in the text, a temperature, peak column density and mass were derived, and these are also listed. The uncertainty in the masses could be as high as a factor of 2. A mean volume density is given, assuming each core is spherical, within the given radius. Finally, a virial mass for each core is estimated using CO and HCO+ linewidths.

into three components in the 160-μm data. The mean off-source pixel-by-pixel 1-σ variation on the $N(H_2)$ map varies from 1.2 to 1.5×10^{21} cm^{-2}. Hence, we adopt a value of 4×10^{21} cm^{-2} for the 3-σ contour.

Five sources are seen in the column density map above a column density of 4×10^{21} cm^{-2}. We here label these cores 1–5 in order of increasing Galactic longitude – see lower right panels of Fig. 1. We list the core positions and their assumed distances in Table 1. The core mentioned above at the bifurcated filament is core 2, and loop 1 contains cores 4 and 5.

The IRAS source IRAS 01432+8725 lies an arcminute to the west of core 4. We believe this offset is sufficient that the two sources are different (the IRAS *FWHM* at 100 μm is 44 arcsec). Therefore, none of the cores is associated with an infrared source, and so these are all candidate starless cores (Myers et al. 1987). The IRAS source is coincident with the centre of the loop, and may in fact be loop 1 itself, as IRAS point sources that only show up at 100 μm have often in the past been shown to be simply bits of cirrus. The *Spitzer* source may be foreground, as it is only seen at the shortest wavelengths.

The reddest features on the false-colour image are the coldest, and loop 1 shows up clearly as redder than the surroundings. Likewise in the temperature map, the loop shows up as blue, indicating that it is the coldest feature on the map. Cores 4 & 5 appear to be the densest features on the map, with peak column densities in excess of 10^{22} cm^{-2}. The column density contour of 4×10^{21} was selected as the core boundary in each case. The radial sizes of the cores were estimated from the images as the equivalent radius of a circle with an area equal to that contained by the core boundary. The derived equivalent radii are listed in Table 1. Flux densities were measured within the core boundary contour in each case, and these are also listed in Table 1.

4. Core properties

The core properties were estimated from the maps of column density and temperature. The flux densities of the pixels coincident with the column density peaks of each core are plotted on the spectral energy distributions (SEDs) shown in Fig. 2. Modified blackbody curves were fitted to the flux densities, and these are also shown in Fig. 2. These are the same fits that were used, pixel-by-pixel, to construct the column density and temperature maps shown in Fig. 1. The form of the fit (cf. Hildebrand 1983) that was used in each case is

$$F_\nu = \Omega B_\nu(T)(m_{\rm H}\mu N(H_2)\kappa_\nu), \quad (1)$$

where F_ν is the flux density at frequency ν, Ω is the solid angle of each pixel, $B_\nu(T)$ is the blackbody function at temperature T, $m_{\rm H}\mu$ is the mean particle mass ($m_{\rm H}$ is the mass of a hydrogen atom and μ was taken to be 2.86, assuming the gas is ~70% H_2 by mass), $N(H_2)$ is the column number density of molecular hydrogen, and κ_ν is the dust mass opacity.

We used the pixel-by-pixel SED fits to calculate the column densities, and hence the core masses. The value of κ_ν that should be used has been the subject of much controversy. Here we adopt the dust opacity recommended by Henning et al. (1995) and Preibisch et al. (1993) for clouds of intermediate density – $n(H_2) \le 10^5$ cm^{-3} – and we assume a standard gas to dust mass ratio of 100. This is a similar parameterization of the dust opacity to that used by Beckwith et al. (1990), namely that

$$\kappa_\nu = 0.1\ {\rm cm^2\ g^{-1}} \times (\nu/1000\ {\rm GHz})^\beta, \quad (2)$$

where we have set the dust opacity index β to be equal to 2.

This is also consistent with the value used by André et al. (1993, 1996) and by Kirk et al. (2005) for prestellar and starless cores. The peak column densities and the temperature at the peak are listed in Table 1. The mass of each core was calculated

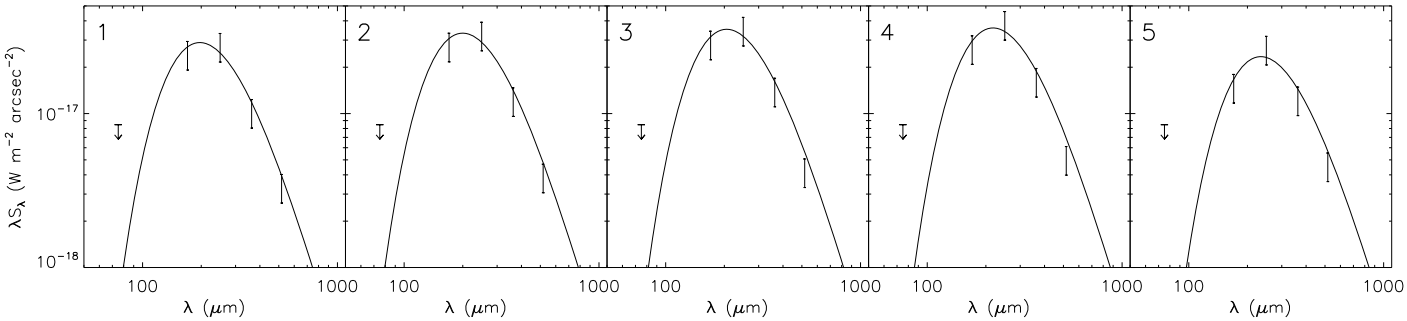

Fig. 2. Spectral energy distributions of cores 1 to 5. The peak flux density in a single 10×10 arcsec pixel was measured. This is shown on a log-log plot of λS_λ versus λ. The data are shown with 15% uncertainty error-bars. The upper limits at 70 μm are shown as arrows. The solid lines are grey-body fits of the form described in the text. The temperatures of the fits are listed in Table 1.

by integrating the column density map within the selected core boundary. This is also listed in Table 1. From these, the volume densities were calculated, assuming that the cores are spherical. These, too, are listed in Table 1.

The temperatures of the SEDs are listed in Table 1. These are all quite low, with values of 10–12 K. This, and the lack of NIR emission from the cores, implies that the star formation process has yet to begin within these particular cores. Hence they are starless cores. This means that these cores should have no internal heating and should be heated solely by the external radiation field. This is similar to what is seen in other low-mass starless and prestellar cores (e.g. Ward-Thompson et al. 2002; or for a review see Ward-Thompson et al. 2007).

Core 5 was observed in the submillimetre by Bernard et al. (1999). Our results are consistent with their findings, allowing for the very different resolutions of the two sets of observations. Falgarone et al. (2009) measured the mean CO linewidths in MCLD 123. For so-called "bright" regions (i.e. high column densities) they found a mean linewidth of 0.4 kms^{-1} in this region. Heithausen et al. (2008) observed MCLD 123 in a number of transitions and found mean linewidths from 0.2 to 0.4 kms^{-1}. Using this range of values we estimated a range of values for the virial masses of the five cores, and list these in Table 1.

We note that all of the cores have masses that are below the virial masses that we have estimated. However, given the uncertainties in the mass calculations, they could be consistent with the lower limit of the range of virial masses. Hence, we can only say that they may or may not be gravitationally bound, and these 5 cores may be on the edge of possibly becoming prestellar cores. Note that this is very different from the cores found in the Aquila region (André et al. 2010), a large fraction of which are clearly gravitationally bound – cf. Fig. 4 of André et al. (2010). Nevertheless, bound or unbound, the 5 cores we have selected are the closest to being gravitationally bound of any of the starless cores in Polaris.

5. Conclusions

We have presented *Herschel* data of the Polaris Flare dark cloud region, and in particular the region MCLD 123. We found a great deal of extended emission at wavelengths from 70 to 500 μm with both PACS and SPIRE. We noted some filamentary and low-level structure. We identified the five densest cores within this structure. We carried out a temperature, mass and density analysis of the cores. We compared their observed masses to their virial masses, and found that the observed masses are on the lower limit of the range of their estimated virial masses, and thus we cannot say for certain whether they are gravitationally bound.

Acknowledgements. J.M.K. acknowledges STFC for funding, while this work was carried out, under the auspices of the Cardiff Astronomy Rolling Grant. SPIRE was developed by a consortium of institutes led by Cardiff Univ. (UK) and including Univ. Lethbridge (Canada); NAOC (China); CEA, LAM (France); IFSI, Univ. Padua (Italy); IAC (Spain); Stockholm Observatory (Sweden); Imperial College London, RAL, UCL-MSSL, UKATC, Univ. Sussex (UK); Caltech, JPL, NHSC, Univ. Colorado (USA). This development has been supported by national funding agencies: CSA (Canada); NAOC (China); CEA, CNES, CNRS (France); ASI (Italy); MCINN (Spain); Stockholm Observatory (Sweden); STFC (UK); and NASA (USA). PACS was developed by a consortium of institutes led by MPE (Germany) and including UVIE (Austria); KUL, CSL, IMEC (Belgium); CEA, LAM (France); MPIA (Germany); IFSI, OAP/AOT, OAA/CAISMI, LENS, SISSA (Italy); IAC (Spain). This development has been supported by the funding agencies BMVIT (Austria), ESA-PRODEX (Belgium), CEA/CNES (France), DLR (Germany), ASI (Italy), and CICT/MCT (Spain).

References

André, P., Ward-Thompson, D., & Barsony, M. 1993, ApJ, 406, 122
André, P., Ward-Thompson, D., & Motte, F. 1996, A&A, 314, 625
André, Ph., et al. 2010, A&A, 518, L102
Beckwith, S. V., Sargent, A. I., Chini, R. S., & Guesten, R. 1990, AJ, 99, 924
Bensch, F., Leuenhagen, U., Stutzki, J., & Schieder, R. 2003, ApJ, 591, 1013
Bernard, J. P., Abergel, A., Ristorcelli, I., et al. 1999, A&A, 347, 640
Falgarone, E., Panis, J. F., & Heithausen A. 1998, A&A, 331, 669
Falgarone, E., Pety, J., & Hily-Blant, P. 2009, A&A, 507, 355
Griffin, M. J., et al. 2010, 518, L3
Grossmann, V., & Heithausen, A. 1992, A&A, 264, 195
Grossmann, V., Meyerdierks, H., Mebold, U., & Heithausen, A. 1990, A&A, 240, 400
Heithausen, A., & Thaddeus, P. 1990, ApJ, 353, L49
Heithausen, A., Bottner, C., & Walter, F. 2008, A&A, 488, 597
Henning, T., Michel, B., & Stognienko, R. 1995, P&SS, 43, 1333
Hildebrand, R. 1983, QJRAS, 24, 267
Kirk, J. M., Ward-Thompson, D., & André, P. 2005, MNRAS, 360, 1506
Kirk, J. M., Ward-Thompson, D., Di Francesco, J., et al. 2009, ApJS, 185, 198
Low, F. J., Young, E., Beintema, D. A., et al. 1984, ApJ, 278, L19
Myers, P. C., Fuller, G. A., Mathieu, R. D., et al. 1987, ApJ, 319, 340
Pilbratt, G. L., et al. 2010, A&A, 518, L1
Poglitsch, A., et al. 2010, A&A, 518, L2
Preibisch, T., Ossenkopf, V., Yorke, H., & Henning, T. 1993, A&A, 279, 577
Ward-Thompson, D., André, P., & Kirk, J. M. 2002, MNRAS, 329, 257
Ward-Thompson, D., et al. 2007, in Protostars & Planets V, 33

Page 5 is available in the electronic edition of the journal at http://www.aanda.org

[1] School of Physics and Astronomy, Cardiff University, Queens Buildings, The Parade, Cardiff, CF243AA, UK
[2] Laboratoire AIM, CEA/DSM-CNRS-Université Paris Diderot, IRFU/ Service d'Astrophysique, C.E. Saclay, Orme des Merisiers, 91191 Gif-sur-Yvette, France
[3] INAF-IFSI, Fosso del Cavaliere 100, 00133 Roma, Italy
[4] IAS, Université Paris-Sud, Bât. 121, 91405 Orsay, France
[5] LAM/OAMP, Université de Provence, 13388 Marseille, France
[6] CESR, 9 Avenue du Colonel Roche, BP 4346, 31029 Toulouse, France
[7] CDS, Observatoire de Strasbourg, 11 rue de l'Université, 67000 Strasbourg, France
[8] IRAM, 300 rue de la Piscine, Domaine Universitaire, 38406 Saint Martin d'Héres, France
[9] Herzberg Institute of Astrophysics, Department of Physics and Astronomy, University of Victoria, Victoria, Canada
[10] NAOC, Chinese Academy of Sciences, A20 Datun Road, Chaoyang District, Beijing 100012, PR China
[11] CITA, University of Toronto, 60 St George Street, Toronto, Ontario, M5S 3H8, Canada
[12] Department of Astronomy, Stockholm University, AlbaNova University Center, 10691 Stockholm, Sweden
[13] UKATC, Royal Observatory, Blackford Hill, Edinburgh, EH93HJ, UK
[14] INAF, Largo Enrico Fermi 5, 50125 Firenze, Italy
[15] RAL, Chilton, Didcot, OX110NL, UK
[16] Dept. of Physics & Astronomy, Open University, Milton Keynes MK7 6AA, UK
[17] Dept. of Physics & Astronomy, McMaster University, Hamilton, Ontario, L8S 4M1, Canada